This document was prepared by the DUNE collaboration using the resources of the Fermi National Accelerator Laboratory (Fermilab), a U.S. Department of Energy, Office of Science, HEP User Facility. Fermilab is managed by Fermi Research Alliance, LLC (FRA), acting under Contract No. DE-AC02-07CH11359.

The DUNE collaboration also acknowledges the international, national, and regional funding agencies supporting the institutions who have contributed to completing this Technical Design Report.

Authors

B. Abi,[129] R. Acciarri,[56] Mario A. Acero,[8] G. Adamov,[59] D. Adams,[15] M. Adinolfi,[14] Z. Ahmad,[163] J. Ahmed,[166] T. Alion,[153] S. Alonso Monsalve,[18] C. Alt,[49] J. Anderson,[4] C. Andreopoulos,[109] M. P. Andrews,[56] F. Andrianala,[2] S. Andringa,[103] A. Ankowski,[143] J. Anthony,[28] M. Antonova,[72] S. Antusch,[9] A. Aranda Fernandez,[36] A. Ariga,[10] L. O. Arnold,[39] M. A. Arroyave,[48] J. Asaadi,[157] A. Aurisano,[34] V. Aushev,[101] D. Autiero,[81] F. Azfar,[129] H. Back,[130] J. J. Back,[166] C. Backhouse,[161] P. Baesso,[14] L. Bagby,[56] R. Bajou,[1] S. Balasubramanian,[170] P. Baldi,[23] B. Bambah,[70] F. Barao,[103, 105] G. Barenboim,[72] G. J. Barker,[166] W. Barkhouse,[123] C. Barnes,[116] G. Barr,[129] J. Barranco Monarca,[64] N. Barros,[103, 106] J. L. Barrow,[155, 56] A. Bashyal,[128] V. Basque,[114] F. Bay,[122] J. L. Bazo Alba,[137] J. F. Beacom,[127] E. Bechetoille,[81] B. Behera,[38] L. Bellantoni,[56] G. Bellettini,[135] V. Bellini,[74] O. Beltramello,[18] D. Belver,[19] N. Benekos,[18] F. Bento Neves,[104] J. Berger,[136] S. Berkman,[56] P. Bernardini,[144] R. M. Berner,[10] H. Berns,[22] S. Bertolucci,[73] M. Betancourt,[56] Y. Bezawada,[22] M. Bhattacharjee,[86] B. Bhuyan,[86] S. Biagi,[152] J. Bian,[23] M. Biassoni,[76] K. Biery,[56] B. Bilki,[11] M. Bishai,[15] A. Bitadze,[114] A. Blake,[107] B. Blanco Siffert,[55] F. D. M. Blaszczyk,[56] G. C. Blazey,[124] E. Blucher,[32] J. Boissevain,[110] S. Bolognesi,[17] T. Bolton,[98] M. Bonesini,[76] M. Bongrand,[102] F. Bonini,[15] A. Booth,[153] C. Booth,[146] S. Bordoni,[18] A. Borkum,[153] T. Boschi,[47] N. Bostan,[90] P. Bour,[41] S. B. Boyd,[166] D. Boyden,[124] J. Bracinik,[12] D. Braga,[56] D. Brailsford,[107] A. Brandt,[157] J. Bremer,[18] C. Brew,[142] E. Brianne,[114] S. J. Brice,[56] C. Brizzolari,[76] C. Bromberg,[117] G. Brooijmans,[39] J. Brooke,[14] A. Bross,[56] G. Brunetti,[131] N. Buchanan,[38] H. Budd,[140] D. Caiulo,[81] P. Calafiura,[108] J. Calcutt,[117] M. Calin,[16] S. Calvez,[38] E. Calvo,[19] L. Camilleri,[39] A. Caminata,[75] M. Campanelli,[161] D. Caratelli,[56] G. Carini,[15] B. Carlus,[81] P. Carniti,[76] I. Caro Terrazas,[38] H. Carranza,[157] A. Castillo,[145] C. Castromonte,[89] C. Cattadori,[76] F. Cavalier,[102] F. Cavanna,[56] S. Centro,[131] G. Cerati,[56] A. Cervelli,[73] A. Cervera Villanueva,[72] M. Chalifour,[18] C. Chang,[25] E. Chardonnet,[1] A. Chatterjee,[136] S. Chattopadhyay,[163] J. Chaves,[132] H. Chen,[15] M. Chen,[23] Y. Chen,[10] D. Cherdack,[69] C. Chi,[39] S. Childress,[56] A. Chiriacescu,[16] K. Cho,[97] S. Choubey,[66] A. Christensen,[38] D. Christian,[56] G. Christodoulou,[18] E. Church,[130] P. Clarke,[50] T. E. Coan,[150] A. G. Cocco,[78] J. A. B. Coelho,[102] E. Conley,[46] J. M. Conrad,[115] M. Convery,[143] L. Corwin,[147] P. Cotte,[17] L. Cremaldi,[119] L. Cremonesi,[161] J. I. Crespo-Anadón,[39] E. Cristaldo,[6] R. Cross,[107] C. Cuesta,[19] Y. Cui,[25] D. Cussans,[14] M. Dabrowski,[15] H. da Motta,[30] L. Da Silva Peres,[55] Q. David,[81] G. S. Davies,[119] S. Davini,[75] J. Dawson,[1] K. De,[157] R. M. De Almeida,[58] P. Debbins,[90] I. De Bonis,[20] M. P. Decowski,[122] A. de Gouvêa,[125] P. C. De Holanda,[29] I. L. De Icaza Astiz,[153] A. Deisting,[85] P. De Jong,[122] A. Delbart,[17] D. Delepine,[64] M. Delgado,[3] A. Dell'Acqua,[18] P. De Lurgio,[4] J. R. T. de Mello Neto,[55] D. M. DeMuth,[162] S. Dennis,[109] C. Densham,[142] G. Deptuch,[56] A. De Roeck,[18] V. De Romeri,[72] J. J. De Vries,[28] R. Dharmapalan,[68] F. Diaz,[137] J. S. Díaz,[88] S. Di Domizio,[75] L. Di Giulio,[18] P. Ding,[56] L. Di Noto,[75] C. Distefano,[152] R. Diurba,[160] M. Diwan,[15] Z. Djurcic,[4] N. Dokania,[151] M. J. Dolinski,[45] L. Domine,[143] D. Douglas,[117] F. Drielsma,[143] D. Duchesneau,[20] K. Duffy,[56] P. Dunne,[85] T. Durkin,[142] H. Duyang,[149] O. Dvornikov,[68] D. A. Dwyer,[108] A. S. Dyshkant,[124] M. Eads,[124] D. Edmunds,[117] J. Eisch,[91] S. Emery,[17] A. Ereditato,[10] C. O. Escobar,[56] L. Escudero Sanchez,[28] J. J. Evans,[114] K. Ewart,[88] A. C. Ezeribe,[146] K. Fahey,[56] A. Falcone,[76] C. Farnese,[131] Y. Farzan,[82] J. Felix,[64] E. Fernandez-Martinez,[113] P. Fernandez Menendez,[72] F. Ferraro,[75] L. Fields,[56] A. Filkins,[168] F. Filthaut,[122] R. S. Fitzpatrick,[116] W. Flanagan,[43] B. Fleming,[170] R. Flight,[140] J. Fowler,[46] W. Fox,[88] J. Franc,[41] K. Francis,[124] D. Franco,[170] J. Freeman,[56] J. Freestone,[114] J. Fried,[15] A. Friedland,[143] S. Fuess,[56] I. Furic,[57] A. P. Furmanski,[160] A. Gago,[137] H. Gallagher,[159] A. Gallego-Ros,[19] N. Gallice,[77, 76] V. Galymov,[81] E. Gamberini,[18] T. Gamble,[146] R. Gandhi,[66] R. Gandrajula,[117] S. Gao,[15] D. Garcia-Gamez,[62] M. Á. García-Peris,[72] S. Gardiner,[56] D. Gastler,[13] G. Ge,[39] B. Gelli,[29] A. Gendotti,[49] S. Gent,[148] Z. Ghorbani-Moghaddam,[75] D. Gibin,[131] I. Gil-Botella,[19] C. Girerd,[81] A. K. Giri,[87] D. Gnani,[108] O. Gogota,[101] M. Gold,[120] S. Gollapinni,[110] K. Gollwitzer,[56] R. A. Gomes,[52] L. V. Gomez Bermeo,[145] L. S. Gomez Fajardo,[145] F. Gonnella,[12] J. A. Gonzalez-Cuevas,[6] M. C. Goodman,[4] O. Goodwin,[114] S. Goswami,[134] C. Gotti,[76] E. Goudzovski,[12] C. Grace,[108] M. Graham,[143] E. Gramellini,[170] R. Gran,[118] E. Granados,[64] A. Grant,[44] C. Grant,[13] D. Gratieri,[58] P. Green,[114] S. Green,[28] L. Greenler,[169] M. Greenwood,[128] J. Greer,[14] W. C. Griffith,[153] M. Groh,[88] J. Grudzinski,[4] K. Grzelak,[165] W. Gu,[15] V. Guarino,[4] R. Guenette,[67] A. Guglielmi,[131] B. Guo,[149] K. K. Guthikonda,[65] R. Gutierrez,[3] P. Guzowski,[114] M. M. Guzzo,[29] S. Gwon,[33] A. Habig,[118] A. Hackenburg,[170] H. Hadavand,[157] R. Haenni,[10] A. Hahn,[56] J. Haigh,[166] J. Haiston,[147] T. Hamernik,[56] P. Hamilton,[85] J. Han,[136] K. Harder,[142] D. A. Harris,[172, 56] J. Hartnell,[153] T. Hasegawa,[96] R. Hatcher,[56] E. Hazen,[13] A. Heavey,[56] K. M. Heeger,[170] K. Hennessy,[109] S. Henry,[140] M. A. Hernandez Morquecho,[64] K. Herner,[56] L. Hertel,[23] A. S. Hesam,[18] J. Hewes,[34] A. Higuera,[69] T. Hill,[83] S. J. Hillier,[12] A. Himmel,[56] J. Hoff,[56] C. Hohl,[9] A. Holin,[161] E. Hoppe,[130] G. A. Horton-Smith,[98] M. Hostert,[47] A. Hourlier,[115] B. Howard,[88] R. Howell,[140] J. Huang,[158] J. Huang,[22] J. Hugon,[111] G. Iles,[85] A. M. Iliescu,[73] R. Illingworth,[56] A. Ioannisian,[171] R. Itay,[143]

A. Izmaylov,[72] E. James,[56] B. Jargowsky,[23] F. Jediny,[41] C. Jesús-Valls,[71] X. Ji,[15] L. Jiang,[164] S. Jiménez,[19] A. Jipa,[16] A. Joglekar,[25] C. Johnson,[38] R. Johnson,[34] B. Jones,[157] S. Jones,[161] C. K. Jung,[151] T. Junk,[56] Y. Jwa,[39] M. Kabirnezhad,[129] A. Kaboth,[142] I. Kadenko,[101] F. Kamiya,[54] G. Karagiorgi,[39] A. Karcher,[108] M. Karolak,[17] Y. Karyotakis,[20] S. Kasai,[100] S. P. Kasetti,[111] L. Kashur,[38] N. Kazaryan,[171] E. Kearns,[13] P. Keener,[132] K.J. Kelly,[56] E. Kemp,[29] W. Ketchum,[56] S. H. Kettell,[15] M. Khabibullin,[80] A. Khotjantsev,[80] A. Khvedelidze,[59] D. Kim,[18] B. King,[56] B. Kirby,[15] M. Kirby,[56] J. Klein,[132] K. Koehler,[169] L. W. Koerner,[69] S. Kohn,[21,108] P. P. Koller,[10] M. Kordosky,[168] T. Kosc,[81] U. Kose,[18] V. A. Kostelecký,[88] K. Kothekar,[14] F. Krennrich,[91] I. Kreslo,[10] Y. Kudenko,[80] V. A. Kudryavtsev,[146] S. Kulagin,[80] J. Kumar,[68] R. Kumar,[139] C. Kuruppu,[149] V. Kus,[41] T. Kutter,[111] A. Lambert,[108] K. Lande,[132] C. E. Lane,[45] K. Lang,[158] T. Langford,[170] P. Lasorak,[153] D. Last,[132] C. Lastoria,[19] A. Laundrie,[169] A. Lawrence,[108] I. Lazanu,[16] R. LaZur,[38] T. Le,[159] J. Learned,[68] P. LeBrun,[81] G. Lehmann Miotto,[18] R. Lehnert,[88] M. A. Leigui de Oliveira,[54] M. Leitner,[108] M. Leyton,[71] L. Li,[23] S. Li,[15] S. W. Li,[143] T. Li,[50] Y. Li,[15] H. Liao,[98] C. S. Lin,[108] S. Lin,[38] A. Lister,[169] B. R. Littlejohn,[84] J. Liu,[23] S. Lockwitz,[56] T. Loew,[108] M. Lokajicek,[40] I. Lomidze,[59] K. Long,[85] K. Loo,[95] D. Lorca,[10] T. Lord,[166] J. M. LoSecco,[126] W. C. Louis,[110] K.B. Luk,[21,108] X. Luo,[26] N. Lurkin,[12] T. Lux,[71] V. P. Luzio,[54] D. MacFarland,[143] A. A. Machado,[29] P. Machado,[56] C. T. Macias,[88] J. R. Macier,[56] A. Maddalena,[61] P. Madigan,[21,108] S. Magill,[4] K. Mahn,[117] A. Maio,[103,106] J. A. Maloney,[42] G. Mandrioli,[73] J. C. Maneira,[103,106] L. Manenti,[161] S. Manly,[140] A. Mann,[159] K. Manolopoulos,[142] M. Manrique Plata,[88] A. Marchionni,[56] W. Marciano,[15] D. Marfatia,[68] C. Mariani,[164] J. Maricic,[68] F. Marinho,[53] A. D. Marino,[37] M. Marshak,[160] C. Marshall,[108] J. Marshall,[166] J. Marteau,[81] J. Martin-Albo,[72] N. Martinez,[138] D.A. Martinez Caicedo,[147] S. Martynenko,[151] K. Mason,[159] A. T. Mastbaum,[141] M. Masud,[72] S. Matsuno,[68] J. Matthews,[111] C. Mauger,[132] N. Mauri,[73] K. Mavrokoridis,[109] R. Mazza,[76] A. Mazzacane,[56] E. Mazzucato,[17] E. McCluskey,[56] N. McConkey,[114] K. S. McFarland,[140] C. McGrew,[151] A. McNab,[114] A. Mefodiev,[80] P. Mehta,[94] P. Melas,[7] M. Mellinato,[76] O. Mena,[72] S. Menary,[172] L. Mendes Santos,[29] H. Mendez,[138] A. Menegolli,[79] G. Meng,[131] M. D. Messier,[88] W. Metcalf,[111] M. Mewes,[88] H. Meyer,[167] T. Miao,[56] G. Michna,[148] T. Miedema,[122] J. Migenda,[146] R. Milincic,[68] W. Miller,[160] J. Mills,[159] C. Milne,[83] O. Mineev,[80] O. G. Miranda,[35] S. Miryala,[15] C. S. Mishra,[56] S. R. Mishra,[149] A. Mislivec,[160] D. Mladenov,[18] I. Mocioiu,[133] K. Moffat,[47] N. Moggi,[73] R. Mohanta,[70] T. A. Mohayai,[56] N. Mokhov,[56] J. Molina,[6] L. Molina Bueno,[49] A. Montanari,[73] C. Montanari,[79] D. Montanari,[56] L. M. Montano Zetina,[35] J. Moon,[115] M. Mooney,[38] A. Moor,[28] D. Moreno,[3] B. Morgan,[166] C. Morris,[69] C. Mossey,[56] E. Motuk,[161] C. A. Moura,[54] J. Mousseau,[116] W. Mu,[56] L. Mualem,[27] J. Mueller,[38] M. Muether,[167] S. Mufson,[88] F. Muheim,[50] A. Muir,[44] M. Mulhearn,[22] H. Muramatsu,[160] S. Murphy,[49] J. Musser,[88] J. Nachtman,[90] S. Nagu,[112] M. Nalbandyan,[171] R. Nandakumar,[142] D. Naples,[136] S. Narita,[92] D. Navas-Nicolás,[19] N. Nayak,[23] M. Nebot-Guinot,[50] L. Necib,[27] K. Negishi,[92] J. K. Nelson,[168] J. Nesbit,[169] M. Nessi,[18] D. Newbold,[142] M. Newcomer,[132] D. Newhart,[56] R. Nichol,[161] E. Niner,[56] K. Nishimura,[68] A. Norman,[56] R. Northrop,[32] P. Novella,[72] J. A. Nowak,[107] M. Oberling,[4] A. Olivares Del Campo,[47] A. Olivier,[140] Y. Onel,[90] Y. Onishchuk,[101] J. Ott,[23] L. Pagani,[22] S. Pakvasa,[68] O. Palamara,[56] S. Palestini,[18] J. M. Paley,[56] M. Pallavicini,[75] C. Palomares,[19] E. Pantic,[22] V. Paolone,[136] V. Papadimitriou,[56] R. Papaleo,[152] A. Papanestis,[142] S. Paramesvaran,[14] S. Parke,[56] Z. Parsa,[15] M. Parvu,[16] S. Pascoli,[47] L. Pasqualini,[73] J. Pasternak,[85] J. Pater,[114] C. Patrick,[161] L. Patrizii,[73] R. B. Patterson,[27] S. J. Patton,[108] T. Patzak,[1] A. Paudel,[98] B. Paulos,[169] L. Paulucci,[54] Z. Pavlovic,[56] G. Pawloski,[160] D. Payne,[109] V. Pec,[146] S. J. M. Peeters,[153] Y. Penichot,[17] E. Pennacchio,[81] A. Penzo,[90] O. L. G. Peres,[29] J. Perry,[50] D. Pershey,[46] G. Pessina,[76] G. Petrillo,[143] C. Petta,[74] R. Petti,[149] F. Piastra,[10] L. Pickering,[117] F. Pietropaolo,[18,131] J. Pillow,[166] R. Plunkett,[56] R. Poling,[160] X. Pons,[18] N. Poonthottathil,[91] S. Pordes,[56] M. Potekhin,[15] R. Potenza,[74] B. V. K. S. Potukuchi,[93] J. Pozimski,[85] M. Pozzato,[73] S. Prakash,[29] T. Prakash,[108] S. Prince,[67] D. Pugnere,[81] K. Qi,[151] X. Qian,[15] J. L. Raaf,[56] R. Raboanary,[2] V. Radeka,[15] J. Rademacker,[14] B. Radics,[49] A. Rafique,[4] E. Raguzin,[15] M. Rai,[166] M. Rajaoalisoa,[34] I. Rakhno,[56] H. T. Rakotondramanana,[2] L. Rakotondravohitra,[2] Y. A. Ramachers,[166] R. Rameika,[56] M. A. Ramirez Delgado,[64] B. Ramson,[56] A. Rappoldi,[79] G. Raselli,[79] P. Ratoff,[107] S. Ravat,[18] H. Razafinime,[2] J.S. Real,[63] B. Rebel,[169,56] D. Redondo,[19] M. Reggiani-Guzzo,[29] T. Rehak,[45] J. Reichenbacher,[147] S. D. Reitzner,[56] A. Renshaw,[69] S. Rescia,[15] F. Resnati,[18] A. Reynolds,[129] G. Riccobene,[152] L. C. J. Rice,[136] K. Rielage,[110] Y. Rigaut,[49] D. Rivera,[132] L. Rochester,[143] M. Roda,[109] P. Rodrigues,[129] M. J. Rodriguez Alonso,[18] J. Rodriguez Rondon,[147] A. J. Roeth,[46] H. Rogers,[38] S. Rosauro-Alcaraz,[113] M. Rossella,[79] J. Rout,[94] S. Roy,[66] A. Rubbia,[49] C. Rubbia,[60] B. Russell,[108] J. Russell,[143] D. Ruterbories,[140] R. Saakyan,[161] S. Sacerdoti,[1] T. Safford,[117] N. Sahu,[87] P. Sala,[77,18] N. Samios,[15] M. C. Sanchez,[91] D. A. Sanders,[119] D. Sankey,[142] S. Santana,[138] M. Santos-Maldonado,[138] N. Saoulidou,[7] P. Sapienza,[152] C. Sarasty,[34] I. Sarcevic,[5] G. Savage,[56] V. Savinov,[136] A. Scaramelli,[79] A. Scarff,[146] A. Scarpelli,[1]

T. Schaffer,[118] H. Schellman,[128,56] P. Schlabach,[56] D. Schmitz,[32] K. Scholberg,[46] A. Schukraft,[56] E. Segreto,[29] J. Sensenig,[132] I. Seong,[23] A. Sergi,[12] F. Sergiampietri,[151] D. Sgalaberna,[18] M. H. Shaevitz,[39] S. Shafaq,[94] M. Shamma,[25] H. R. Sharma,[93] R. Sharma,[15] T. Shaw,[56] C. Shepherd-Themistocleous,[142] S. Shin,[32] D. Shooltz,[117] R. Shrock,[151] L. Simard,[102] N. Simos,[15] J. Sinclair,[10] G. Sinev,[46] J. Singh,[112] J. Singh,[112] R. Sipos,[18] F. W. Sippach,[39] G. Sirri,[73] A. Sitraka,[147] K. Siyeon,[33] D. Smargianaki,[151] A. Smith,[46] A. Smith,[28] E. Smith,[88] P. Smith,[88] J. Smolik,[41] M. Smy,[23] P. Snopok,[84] M. Soares Nunes,[29] H. Sobel,[23] M. Soderberg,[154] C. J. Solano Salinas,[89] S. Söldner-Rembold,[114] N. Solomey,[167] V. Solovov,[104] W. E. Sondheim,[110] M. Sorel,[72] J. Soto-Oton,[19] A. Sousa,[34] K. Soustruznik,[31] F. Spagliardi,[129] M. Spanu,[15] J. Spitz,[116] N. J. Spooner,[146] K. Spurgeon,[154] R. Staley,[12] M. Stancari,[56] L. Stanco,[131] H. M. Steiner,[108] J. Stewart,[15] B. Stillwell,[32] J. Stock,[147] F. Stocker,[18] T. Stokes,[111] M. Strait,[160] T. Strauss,[56] S. Striganov,[56] A. Stuart,[36] D. Summers,[119] A. Surdo,[144] V. Susic,[9] L. Suter,[56] C. M. Sutera,[74] R. Svoboda,[22] B. Szczerbinska,[156] A. Szelc,[114] R. Talaga,[4] H. A. Tanaka,[143] B. Tapia Oregui,[158] A. Tapper,[85] S. Tariq,[56] E. Tatar,[83] R. Tayloe,[88] A. M. Teklu,[151] M. Tenti,[73] K. Terao,[143] C. A. Ternes,[72] F. Terranova,[76] G. Testera,[75] A. Thea,[142] J. L. Thompson,[146] C. Thorn,[15] S. C. Timm,[56] A. Tonazzo,[1] M. Torti,[76] M. Tortola,[72] F. Tortorici,[74] D. Totani,[56] M. Toups,[56] C. Touramanis,[109] J. Trevor,[27] W. H. Trzaska,[95] Y. T. Tsai,[143] Z. Tsamalaidze,[59] K. V. Tsang,[143] N. Tsverava,[59] S. Tufanli,[18] C. Tull,[108] E. Tyley,[146] M. Tzanov,[111] M. A. Uchida,[28] J. Urheim,[88] T. Usher,[143] M. R. Vagins,[99] P. Vahle,[168] G. A. Valdiviesso,[51] E. Valencia,[168] Z. Vallari,[27] J. W. F. Valle,[72] S. Vallecorsa,[18] R. Van Berg,[132] R. G. Van de Water,[110] D. Vanegas Forero,[29] F. Varanini,[131] D. Vargas,[71] G. Varner,[68] J. Vasel,[88] G. Vasseur,[17] K. Vaziri,[56] S. Ventura,[131] A. Verdugo,[19] S. Vergani,[28] M. A. Vermeulen,[122] M. Verzocchi,[56] H. Vieira de Souza,[29] C. Vignoli,[61] C. Vilela,[151] B. Viren,[15] T. Vrba,[41] T. Wachala,[121] A. V. Waldron,[85] M. Wallbank,[34] H. Wang,[24] J. Wang,[22] Y. Wang,[24] Y. Wang,[151] K. Warburton,[91] D. Warner,[38] M. Wascko,[85] D. Waters,[161] A. Watson,[12] P. Weatherly,[45] A. Weber,[142,129] M. Weber,[10] H. Wei,[15] A. Weinstein,[91] D. Wenman,[169] M. Wetstein,[91] M. R. While,[147] A. White,[157] L. H. Whitehead,[28] D. Whittington,[154] M. J. Wilking,[151] C. Wilkinson,[10] Z. Williams,[157] F. Wilson,[142] R. J. Wilson,[38] J. Wolcott,[159] T. Wongjirad,[159] K. Wood,[151] L. Wood,[130] E. Worcester,[15] M. Worcester,[15] C. Wret,[140] W. Wu,[56] W. Wu,[23] Y. Xiao,[23] G. Yang,[151] T. Yang,[56] N. Yershov,[80] K. Yonehara,[56] T. Young,[123] B. Yu,[15] J. Yu,[157] J. Zalesak,[40] L. Zambelli,[20] B. Zamorano,[62] A. Zani,[77] L. Zazueta,[168] G. P. Zeller,[56] J. Zennamo,[56] K. Zeug,[169] C. Zhang,[15] M. Zhao,[15] E. Zhivun,[15] G. Zhu,[127] E. D. Zimmerman,[37] M. Zito,[17] S. Zucchelli,[73] J. Zuklin,[40] V. Zutshi,[124] and R. Zwaska[56]

(The DUNE Collaboration)

[1] *APC - Université de Paris, CNRS/IN2P3, CEA/lrfu, Observatoire de Paris, 10, rue Alice Domon et Léonie Duquet, 75205 Paris Cedex 13, France*
[2] *University of Antananarivo, BP 566, Antananarivo 101, Madagascar*
[3] *Universidad Antonio Nariño, Cra 3 Este No 47A-15, Bogotá, Colombia*
[4] *Argonne National Laboratory, Argonne, IL 60439, USA*
[5] *University of Arizona, 1118 E. Fourth Street Tucson, AZ 85721, USA*
[6] *Universidad Nacional de Asunción, San Lorenzo, Paraguay*
[7] *University of Athens, University Campus, Zografou GR 157 84, Greece*
[8] *Universidad del Atlantico, Carrera 30 Número 8- 49 Puerto Colombia - Atlántico, Colombia*
[9] *University of Basel, Klingelbergstrasse 82, CH-4056 Basel, Switzerland*
[10] *University of Bern, Sidlerstrasse 5, CH-3012 Bern, Switzerland*
[11] *Beykent University, Istanbul*
[12] *University of Birmingham, Edgbaston, Birmingham B15 2TT, United Kingdom*
[13] *Boston University, Boston, MA 02215, USA*
[14] *University of Bristol, H. H. Wills Physics Laboratory, Tyndall Avenue Bristol BS8 1TL, United Kingdom*
[15] *Brookhaven National Laboratory, Upton, NY 11973, USA*
[16] *University of Bucharest, Faculty of Physics, Bucharest, Romania*
[17] *CEA/Saclay, IRFU Institut de Recherche sur les Lois Fondamentales de l'Univers, F-91191 Gif-sur-Yvette CEDEX, France*
[18] *CERN, European Organization for Nuclear Research 1211 Genève 23, Switzerland, CERN*
[19] *CIEMAT, Centro de Investigaciones Energéticas, Medioambientales y Tecnológicas, Av. Complutense, 40, E-28040 Madrid, Spain*
[20] *Laboratoire d'Annecy-le-Vieux de Physique des Particules, CNRS/IN2P3 and Université Savoie Mont Blanc, CNRS/IN2P3 and Université Savoie Mont Blanc, 74941 Annecy-le-Vieux, France*
[21] *University of California Berkeley, Berkeley, CA 94720, USA*
[22] *University of California Davis, Davis, CA 95616, USA*
[23] *University of California Irvine, Irvine, CA 92697, USA*
[24] *University of California Los Angeles, Los Angeles, CA 90095, USA*
[25] *University of California Riverside, 900 University Ave, Riverside CA 92521*
[26] *University of California Santa Barbara, Santa Barbara, California 93106 USA*

[27]California Institute of Technology, Pasadena, CA 91125, USA
[28]University of Cambridge, JJ Thomson Avenue, Cambridge CB3 0HE, United Kingdom
[29]Universidade Estadual de Campinas, Campinas - SP, 13083-970, Brazil
[30]Centro Brasileiro de Pesquisas Físicas, Rio de Janeiro, RJ 22290-180, Brazil
[31]Institute of Particle and Nuclear Physics of the Faculty of Mathematics and Physics of the Charles University in Prague, V Holešovičkách 747/2, 180 00 Praha 8-Libeň, Czech Republic
[32]University of Chicago, Chicago, IL 60637, USA
[33]Chung-Ang University, Dongjak-Gu, Seoul 06974, South Korea
[34]University of Cincinnati, Cincinnati, OH 45221, USA
[35]Centro de Investigacion y de Estudios Avanzados del IPN (Cinvestav), Mexico City
[36]Universidad de Colima, 340 Colonia Villa San Sebastian Colima, Colima, Mexico
[37]University of Colorado Boulder, Boulder, CO 80309, USA
[38]Colorado State University, Fort Collins, CO 80523, USA
[39]Columbia University, New York, NY 10027, USA
[40]Institute of Physics, Czech Academy of Sciences, Na Slovance 2, 182 21 Praha 8, Czech Republic
[41]Czech Technical University in Prague, Břehová 78/7, 115 19 Prague 1, Czech Republic
[42]Dakota State University, Madison, SD 57042, USA
[43]University of Dallas, Irving, TX 75062-4736, USA
[44]Daresbury Laboratory, Daresbury Warrington, Cheshire WA4 4AD, United Kingdom
[45]Drexel University, Philadelphia, PA 19104, USA
[46]Duke University, Durham, NC 27708, USA
[47]Durham University, South Road, Durham DH1 3LE, United Kingdom
[48]Universidad EIA, Via José María Córdoba #km 2 + 200, Envigado, Antioquia
[49]ETH Zurich, Institute for Particle Physics, Zurich, Switzerland
[50]University of Edinburgh, Edinburgh EH8 9YL, United Kingdom
[51]Universidade Federal de Alfenas, Poços de Caldas - MG, 37715-400, Brazil
[52]Universidade Federal de Goias, Goiania, GO 74690-900, Brazil
[53]Universidade Federal de São Carlos, Araras - SP, 13604-900, Brazil
[54]Universidade Federal do ABC, Av. dos Estados 5001, Santo André - SP, 09210-580 Brazil
[55]Universidade Federal do Rio de Janeiro, Rio de Janeiro - RJ, 21941-901, Brazil
[56]Fermi National Accelerator Laboratory, Batavia, IL 60510
[57]University of Florida, PO Box 118440 Gainesville, FL 32611-8440, USA
[58]Fluminense Federal University, Rua Miguel de Frias, 9 Icaraí Niterói - RJ, 24220-900, Brazil
[59]Georgian Technical University, 77 Kostava Str. 0160, Tbilisi, Georgia
[60]Gran Sasso Science Institute, Viale Francesco Crispi 7, L'Aquila, Italy
[61]Laboratori Nazionali del Gran Sasso, I-67010 Assergi, AQ, Italy
[62]University of Granada & CAFPE, Campus Fuentenueva (Edif. Mecenas), 18002 Granada, Spain
[63]University Grenoble Alpes, CNRS, Grenoble INP, LPSC-IN2P3, 38000 Grenoble, France
[64]Universidad de Guanajuato, Gto., C.P. 37000, Mexico
[65]Department of Physics, K L E F, Green Fields, Guntur - 522 502, AP, India
[66]Harish-Chandra Research Institute, Jhunsi, Allahabad 211 019, India
[67]Harvard University, 17 Oxford St. Cambridge, MA 02138, USA
[68]University of Hawaii, Honolulu, HI 96822, USA
[69]University of Houston, Houston, TX 77204, USA
[70]University of Hyderabad, Gachibowli, Hyderabad - 500 046, India
[71]Institut de Fìsica d'Altes Energies, Barcelona i.e. Catalan ersitat Autonoma de Barcelona, Campus UAB, Facultat Ciències Nord, 08193 Bellaterra, Barcelona, Spain
[72]Instituto de Fisica Corpuscular, Catedratico Jose Beltran, 2 E-46980 Paterna (Valencia), Spain
[73]Istituto Nazionale di Fisica Nucleare Bologna, 40127 Bologna BO, Italy
[74]Istituto Nazionale di Fisica Nucleare Sezione di Catania, Via Santa Sofia 64, I-95123 Catania, Italy
[75]Università degli studi di Genova, Istituto Nazionale di Fisica Nucleare Genova, 16126 Genova GE, Italy
[76]Istituto Nazionale di Fisica Nucleare Sezione di Milano Bicocca and University of Milano Bicocca, Piazza della Scienza, 3 - I-20126 Milano, Italy
[77]Istituto Nazionale di Fisica Nucleare Milano, I-20133 Milano, Italy
[78]Istituto Nazionale di Fisica Nucleare - Sezione di Napoli, Complesso Universitario di Monte S. Angelo, I-80126 Napoli, Italy
[79]Università degli studi di Pavia, Istituto Nazionale di Fisica Nucleare Sezione di Pavia, I-27100 Pavia, Italy
[80]Institute for Nuclear Research of the Russian Academy of Sciences , prospekt 60-letiya Oktyabrya 7a, Moscow 117312, Russia
[81]Institut de Physique des 2 Infinis de Lyon, Rue E. Fermi 4 69622 Villeurbanne, France
[82]Institute for Research in Fundamental Sciences , Farmanieh St. Tehran, 19538-33511, Iran
[83]Idaho State University, Department of Physics, Pocatello, ID 83209, USA
[84]Illinois Institute of Technology, Chicago, IL 60616, USA
[85]Imperial College of Science Technology and Medicine, Blackett Laboratory Prince Consort Road, London SW7 2BZ, United Kingdom
[86]Indian Institute of Technology Guwahati, Guwahati, 781 039, India

[87]*Indian Institute of Technology Hyderabad, Hyderabad, 502285, India*
[88]*Indiana University, Bloomington, IN 47405, USA*
[89]*Universidad Nacional de Ingeniería, Av. Tupac Amaru 210, Lima 25, Perú*
[90]*University of Iowa, Department of Physics and Astronomy 203 Van Allen Hall Iowa City, IA 52242, USA*
[91]*Iowa State University, Ames, Iowa 50011, USA*
[92]*Iwate University, Morioka, Iwate 020-8551, Japan*
[93]*University of Jammu, Physics Department, JAMMU-180006, India*
[94]*Jawaharlal Nehru University, School of Physical Sciences, New Delhi 110067, India*
[95]*University of Jyvaskyla, P.O. Box 35, FI-40014, Finland*
[96]*High Energy Accelerator Research Organization (KEK), Ibaraki, 305-0801, Japan*
[97]*Korea Institute of Science and Technology Information, Daejeon, 34141, South Korea*
[98]*Kansas State University, Manhattan, KS 66506, USA*
[99]*Kavli Institute for the Physics and Mathematics of the Universe , Kashiwa, Chiba 277-8583, Japan*
[100]*National Institute of Technology, Kure College, Hiroshima, 737-8506, Japan*
[101]*Kyiv National University, 64, 01601 Kyiv, Ukraine*
[102]*Laboratoire de l'Accélérateur Linéaire , Bâtiment 200, 91440 Orsay, France*
[103]*Laboratório de Instrumentação e Física Experimental de Partículas - LIP, Lisboa, Portugal*
[104]*Laboratório de Instrumentação e Física Experimental de Partículas - LIP, Coimbra, Portugal*
[105]*Instituto Superior Técnico - IST, Universidade de Lisboa, Portugal*
[106]*Faculdade de Ciências - FCUL, Universidade de Lisboa, Portugal*
[107]*Lancaster University, Bailrigg, Lancaster LA1 4YB, United Kingdom*
[108]*Lawrence Berkeley National Laboratory, Berkeley, CA 94720, USA*
[109]*University of Liverpool, L69 7ZE, Liverpool, United Kingdom*
[110]*Los Alamos National Laboratory, Los Alamos, NM 87545, USA*
[111]*Louisiana State University, Baton Rouge, LA 70803, USA*
[112]*University of Lucknow, Lucknow 226007, Uttar Pradesh, India*
[113]*Madrid Autonoma University and IFT UAM/CSIC, Ciudad Universitaria de Cantoblanco 28049 Madrid, Spain*
[114]*University of Manchester, Oxford Road, Manchester M13 9PL, United Kingdom*
[115]*Massachusetts Institute of Technology, Cambridge, MA 02139, USA*
[116]*University of Michigan, Ann Arbor, MI 48109, USA*
[117]*Michigan State University, East Lansing, MI 48824, USA*
[118]*University of Minnesota Duluth, Duluth, MN 55812, USA*
[119]*University of Mississippi, P.O. Box 1848, University, MS 38677 USA*
[120]*University of New Mexico, 1919 Lomas Blvd. N.E. Albuquerque, NM 87131, USA*
[121]*H. Niewodniczański Institute of Nuclear Physics, Polish Academy of Sciences, Cracow, Poland*
[122]*Nikhef National Institute of Subatomic Physics, Science Park, Amsterdam, Netherlands*
[123]*University of North Dakota, 3501 University Ave Grand Forks, ND 58202-8357, USA*
[124]*Northern Illinois University, Department of Physics, DeKalb, Illinois 60115, USA*
[125]*Northwestern University, Evanston, Il 60208, USA*
[126]*University of Notre Dame, Notre Dame, IN 46556, USA*
[127]*Ohio State University, 191 W. Woodruff Ave. Columbus, OH 43210, USA*
[128]*Oregon State University, Corvallis, OR 97331, USA*
[129]*University of Oxford, Oxford, OX1 3RH, United Kingdom*
[130]*Pacific Northwest National Laboratory, Richland, WA 99352, USA*
[131]*Universtà Degli Studi di Padova, Dip. Fisica e Astronomia G. Galilei and INFN Sezione di Padova, I-35131 Padova, Italy*
[132]*University of Pennsylvania, Philadelphia, PA 19104, USA*
[133]*Pennsylvania State University, University Park, PA 16802, USA*
[134]*Physical Research Laboratory, Ahmedabad 380 009, India*
[135]*Università di Pisa, Theor. Division; Largo B. Pontecorvo 3, Ed. B-C, I-56127 Pisa, Italy*
[136]*University of Pittsburgh, Pittsburgh, PA 15260, USA*
[137]*Pontificia Universidad Católica del Perú, Apartado 1761, Lima, Perú*
[138]*University of Puerto Rico, Mayaguez, 00681, USA*
[139]*Punjab Agricultural University, Department of Math. Stat. & Physics, Ludhiana 141004, India*
[140]*University of Rochester, Rochester, NY 14627, USA*
[141]*Rutgers University, Piscataway, NJ, 08854, USA*
[142]*STFC Rutherford Appleton Laboratory, OX11 0QX Harwell Campus, Didcot, United Kingdom*
[143]*SLAC National Acceleratory Laboratory, Menlo Park, CA 94025, USA*
[144]*Università del Salento and Istituto Nazionale Fisica Nucleare, Via Provinciale per Arnesano, 73100 Lecce, Italy*
[145]*Universidad Sergio Arboleda, Cll 74 -14 -14, 11022 Bogotá, Colombia*
[146]*University of Sheffield, Department of Physics and Astronomy, Sheffield S3 7RH, United Kingdom*
[147]*South Dakota School of Mines and Technology, Rapid City, SD 57701, USA*
[148]*South Dakota State University, Brookings, SD 57007, USA*
[149]*University of South Carolina, Columbia, SC 29208, USA*
[150]*Southern Methodist University, Dallas, TX 75275, USA*

[151] *Stony Brook University, SUNY, Stony Brook, New York 11794, USA*
[152] *INFN - Laboratori Nazionali del Sud (LNS), Via S. Sofia 62, 95123 Catania, Italy*
[153] *University of Sussex, Brighton, BN1 9RH, United Kingdom*
[154] *Syracuse University, Syracuse, NY 13244, USA*
[155] *University of Tennessee at Knoxville, TN, 37996, USA*
[156] *Texas A&M University (Corpus Christi), Corpus Christi, TX 78412, USA*
[157] *University of Texas at Arlington, Arlington, TX 76019, USA*
[158] *University of Texas at Austin, Austin, TX 78712, USA*
[159] *Tufts University, Medford, MA 02155, USA*
[160] *University of Minnesota Twin Cities, Minneapolis, MN 55455, USA*
[161] *University College London, London, WC1E 6BT, United Kingdom*
[162] *Valley City State University, Valley City, ND 58072, USA*
[163] *Variable Energy Cyclotron Centre, 1/AF, Bidhannagar Kolkata - 700 064 West Bengal, India*
[164] *Virginia Tech, Blacksburg, VA 24060, USA*
[165] *University of Warsaw, Faculty of Physics ul. Pasteura 5 02-093 Warsaw, Poland*
[166] *University of Warwick, Coventry CV4 7AL, United Kingdom*
[167] *Wichita State University, Physics Division, Wichita, KS 67260, USA*
[168] *William and Mary, Williamsburg, VA 23187, USA*
[169] *University of Wisconsin Madison, Madison, WI 53706, USA*
[170] *Yale University, New Haven, CT 06520, USA*
[171] *Yerevan Institute for Theoretical Physics and Modeling, Halabian Str. 34, Yerevan 0036, Armenia*
[172] *York University, Physics and Astronomy Department, 4700 Keele St. Toronto M3J 1P3, Canada*

Contents

Contents i

List of Figures ii

List of Tables 1

A Roadmap of the DUNE Technical Design Report 1

1 Single-Phase Far Detector Technology 2
- 1.1 Overview . . . 2
- 1.2 Anode Planes . . . 5
- 1.3 Cathode Planes and High Voltage . . . 7
- 1.4 Electronics . . . 7
- 1.5 Photon Detection System . . . 8
- 1.6 Calibration . . . 9
- 1.7 Data Acquisition . . . 10
- 1.8 Cryogenics Instrumentation and Slow Controls . . . 11
- 1.9 Installation . . . 11

Glossary 13

References 18

List of Figures

1.1 A far detector (FD) cryostat 4
1.2 An anode plane assembly (APA) 5
1.3 A stack of two APAs 6
1.4 A section of the field cage (FC) 7
1.5 An X-ARAPUCA photon detector (PD) cell 8
1.6 PD modules mounted in an APA 9

List of Tables

1.1 Key parameters for a 10 kt FD SP module 4

Chapter 1

Single-Phase Far Detector Technology

This chapter provides a brief introduction to the single-phase (SP) far detector technology. The text below closely follows that found in the introductory chapter of Volume IV, The DUNE Far Detector Single-Phase Technology, where many more details may be found.

1.1 Overview

The overriding physics goals of Deep Underground Neutrino Experiment (DUNE) are to search for leptonic charge-parity symmetry violation (CPV) and for nucleon decay as a signature of a grand unified theory (GUT) underlying the standard model (SM), as well as to observe neutrino bursts from supernovae. Central to achieving this physics program is constructing a detector that combines the many-kiloton fiducial mass necessary for rare event searches with sub-centimeter spatial resolution in its ability to image those events, allowing us to identify the signatures of the physics processes we seek among the many backgrounds. The single-phase (SP) liquid argon time-projection chamber (LArTPC) [1] allows us to achieve these dual goals, providing a way to read out with sub-centimeter granularity the patterns of ionization in 10 kt volumes of liquid argon (LAr) resulting from the $O(1\,\text{MeV})$ interactions of solar and supernova neutrinos up to the $O(1\,\text{GeV})$ interactions of neutrinos from the Long-Baseline Neutrino Facility (LBNF) beam.

To search for leptonic CPV, we must study ν_e appearance in the LBNF ν_μ beam. This requires the ability to separate electromagnetic activity induced by charged current (CC) ν_e interactions from similar activity arising from photons, such as photons from π^0 decay. Two signatures allow this. First, photon showers are typically preceded by a gap prior to conversion, characterized by the 18 cm conversion length in LAr. Second, the initial part of a photon shower, where an electron-positron pair is produced, has twice the dE/dx of the initial part of an electron-induced shower. To search for nucleon decay, where the primary channel of interest is $p \to K^+\overline{\nu}$, we must identify kaon tracks as short as a few centimeters. It is also vital to accurately fiducialize these nucleon-decay events to suppress cosmic-muon-induced backgrounds, and here detecting argon-scintillation photons is important in determining the time of the event. Detecting a supernova neutrino burst

(SNB) poses different challenges: those of dealing with a high data rate and maintaining the high detector up-time required to ensure we do not miss one of these rare events. The signature of an SNB is a collection of MeV-energy electron tracks a few centimeters in length from CC ν_e interactions, spread over the entire detector volume. To fully reconstruct an SNB, the entire detector must be read out, a data-rate of up to 2 TB/s, for 30 s to 100 s, including a $\sim$4 s pre-trigger window.

Figure **??** in Section **??** shows a schematic of the general operating principle of a SP LArTPC. A large volume of LAr is subjected to a strong E field of a few hundred volts per centimeter. Charged particles passing through the detector ionize the argon atoms, and the ionization electrons drift in the E field to the anode wall (called an anode plane assembly (APA) array) on a timescale of milliseconds. The SP module APAs consist of layers of active wires strung at angles to each other to form a grid. The relative voltage between the layers is chosen to ensure that all but the final layer are transparent to the drifting electrons, and these first layers produce bipolar induction signals as the electrons pass through them. The final layer collects the drifting electrons, resulting in a monopolar signal.

LAr is also an excellent scintillator, emitting VUV light at a wavelength of 127 nm. This prompt scintillation light, which crosses the detector on a timescale of nanoseconds, is shifted into the visible and collected by photon detectors (PDs). The PDs can provide a t_0 determination for events, indicating when the ionization electrons began to drift. Relative to this t_0, the time at which the ionization electrons reach the anode allows reconstruction of the event topology along the drift direction, which is crucial to fiducialize nucleon-decay events and to apply drift corrections to the ionization charge.

The pattern of current observed on the grid of anode wires provides information for reconstruction in the two coordinates perpendicular to the drift direction. The wire pitch on the wire layers is chosen to optimize considerations of spatial resolution, cost, and signal-to-noise (S/N) of the ionization measurement. S/N is important because the measurement of the ionization collected is a direct measurement of the dE/dx of the charged particles, which is what enables both calorimetry and particle identification (PID).

Figure **??** in Section **??** shows a 10 kt fiducial mass SP module (17.5 kt total mass); the key parameters of a SP module are listed in Table 1.1. Inside a cryostat of outer dimensions 65.8 m (L) by 18.9 m (W) by 17.8 m (H), shown in Figure 1.1, four 3.5 m drift volumes are created between five alternating APA and cathode plane assembly (CPA) arrays, each of dimensions 58.2 m (L) by 12.0 m (H).

The target purity from electronegative contaminants in the argon is $<$100 parts per trillion (ppt) O_2 equivalent, enough to ensure a $>$3 ms ionization-electron lifetime at the nominal 500 V/cm drift voltage. This target electron lifetime ensures S/N of $>$5 for the induction planes and $>$10 for the collection planes, which are necessary to perform pattern recognition and two-track separation.

Nitrogen contamination must be $<$25 parts per million (ppm) to ensure we achieve our requirement of at least 0.5 photoelectrons per MeV detected for events in all parts of the detector, which in turn ensures that we can fiducialize nucleon decay events throughout the detector.

Table 1.1: Key parameters for a 10 kt FD SP module.

Item	Quantity
TPC size	12.0 m × 14.0 m × 58.2 m
Nominal fiducial mass	10 kt
APA size	6 m × 2.3 m
CPA size	1.2 m × 4 m
Number of APAs	150
Number of CPAs	300
Number of X-ARAPUCA PD bars	1500
X-ARAPUCA PD bar size	209 cm × 12 cm × 2 cm
Design voltage	−180 kV
Design drift field	500 V/cm
Drift length	3.5 m
Drift speed	1.6 mm/µs

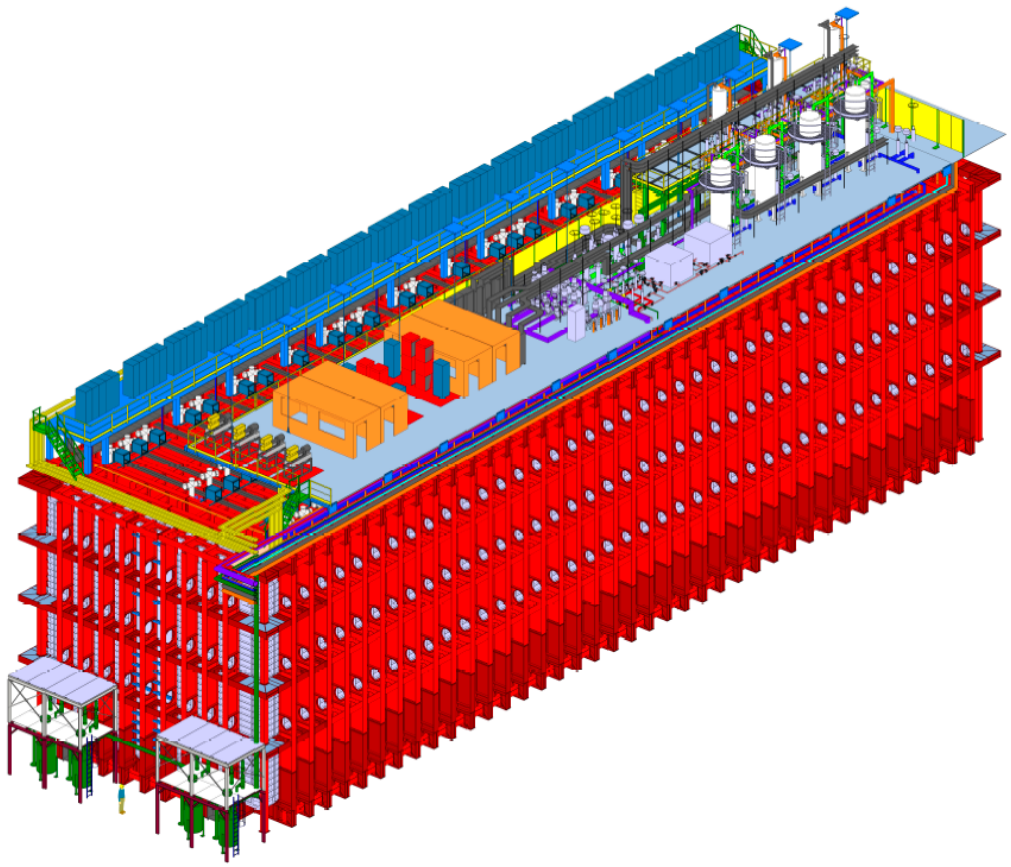


Figure 1.1: A 65.8 m (L) by 18.9 m (W) by 17.8 m (H) outer-dimension cryostat that houses a 10 kt far detector (FD) module. A mezzanine (light blue) installed 2.3 m above the cryostat supports both detector and cryogenics instrumentation. At lower left, between the LAr recirculation pumps (green) installed on the cavern floor, the figure of a person indicates the scale.

1.2 Anode Planes

The modular anode walls are each made up of 50 APAs (25 along the module length and two high), each 6 m × 2.3 m. Figure 1.2 shows a schematic and a photograph. As Figure 1.3 shows, the APAs hang vertically. The APAs are two-sided, with three active wire layers and an additional shielding layer, sometimes called a grid layer, wrapped around them. The wire spacing on the layers is ∼5 mm. The collection layer is called the X layer; the induction layer immediately next to that is called the V layer; the next induction layer is the U layer; and the shielding layer is the G layer. The X and G layer wires run vertically when installed (Figure 1.2 shows them horizontal); the U and V layer wires are at ± 35.7° to the vertical. The wire spacing on each plane defines the spatial resolution of the APA; it is wide enough to keep readout costs low and S/N high, but small enough to enable reconstruction of short tracks such as few-cm kaon tracks from proton decay events.

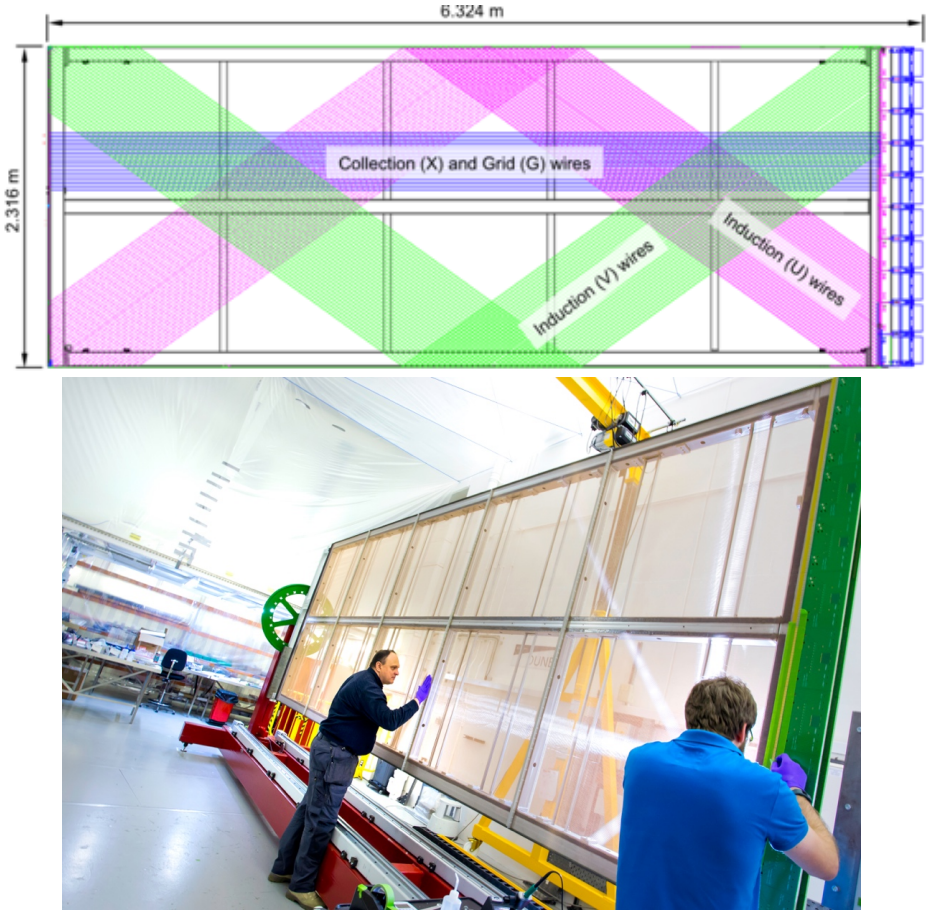


Figure 1.2: Top: a schematic of an APA. The steel APA frame is shown in black. The green and magenta lines indicate the directions of the induction wire layers. The blue lines indicate the directions of the induction and shielding (grid) wire layers. The blue boxes at the right end are the cold electronics (CE). Bottom: a ProtoDUNE-SP APA in a wire-winding machine. The end on the right is the head end, onto which the CE are mounted.

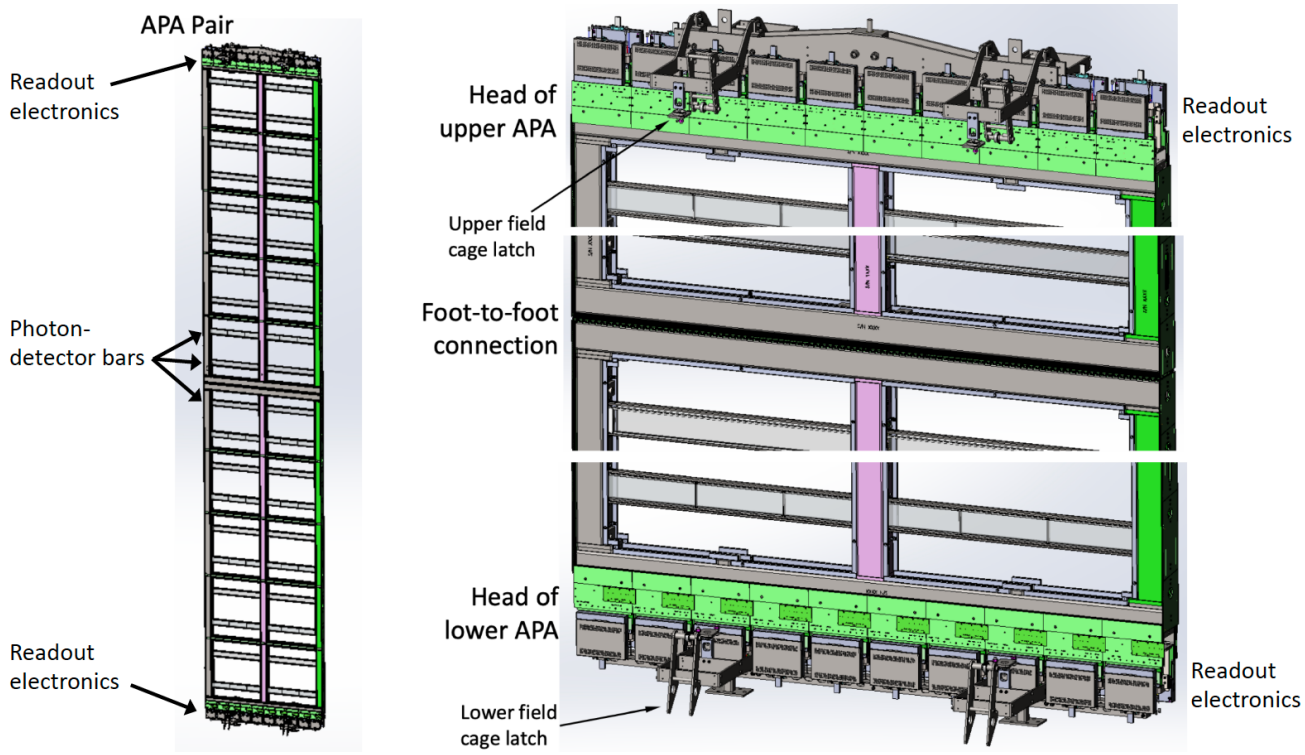


Figure 1.3: Left: two vertically linked APAs form one unit of an APA array. PD bars are installed across the width of the APAs. Right: a zoom into only the top and bottom ends of the APA stack (notice the breaks in white). This shows the readout electronics and the center of the stack where the APAs are connected.

1.3 Cathode Planes and High Voltage

Each of the module's two cathode plane assembly (CPA) arrays is formed from 150 CPAs (50 along the length, stacked three high), each of which is a $1.2\,\mathrm{m} \times 4\,\mathrm{m}$ resistive panel. Each CPA has its own independent high voltage (HV) supply, providing a current of 0.16 mA at $-180\,\mathrm{kV}$. With the APA arrays held close to ground, this results in a uniform $500\,\mathrm{V/cm}$ E field across the drift volume. A typical minimum ionizing particle (MIP) passing through the argon produces roughly 60k ionization electrons per centimeter that drift toward the anodes at approximately $1.6\,\mathrm{mm/\mu s}$. The time to cover the full drift distance is about 2.2 ms.

A field cage (FC) built from field-shaping aluminum profiles surrounds the drift volumes, keeping the E field uniform throughout the active time projection chamber (TPC) volume to within 1%. The aluminum profiles are connected via a resistive divider chain; between each profile, two $5\,\mathrm{G\Omega}$ resistors, arranged in parallel, provide $2.5\,\mathrm{G\Omega}$ resistance to create a nominal 3 kV drop. The FC is illustrated in Figure 1.4.

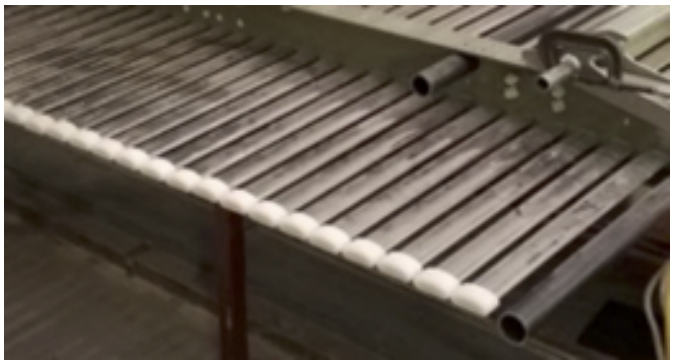


Figure 1.4: A section of the field cage, showing the extruded aluminum field-shaping profiles, with white polyethylene caps on the ends to prevent discharges.

1.4 Electronics

Front-end (FE) readout electronics (in the LAr), called cold electronics (CE), are attached to the top end of the top APA and the bottom end of the bottom APA. Benefitting from a reduction in thermal noise due to the low temperature, the CE shape, amplify, and digitize the signals from the APA induction and collection wires thanks to a series of three different types of ASICs through which all signals pass. Outside the cryostat, signals are passed to warm interface boards (WIBs) that put the signals onto 10 GB optical fibers, ten per APA, which will carry the signals to the upstream data acquisition (DAQ) system in the central utility cavern (CUC). Each detector module has an independent DAQ system that allows it to run as an independent detector, thereby minimizing any chance of a complete FD outage. Modules can, however, provide the others with an SNB trigger signal. The DAQ system also provides the detector clock.

To enable observation of low-energy particles, we plan to keep noise below $1000\,e^-$ per channel, which should be compared to the 20k – 30k e^- per channel collected from a MIP traveling parallel

to the wire plane and perpendicular to the wire orientation. For large signals, we require a linear response up to 500k e^-, which ensures that fewer than 10% of beam events experience saturation. This can be achieved using 12 analog-to-digital converter (ADC) bits. The CE are designed with an FE peaking time of 1 µs, which matches the time for the electrons to drift between wire planes on the APA; this leads to a design sampling frequency of 2 MHz to satisfy the Nyquist criterion.

1.5 Photon Detection System

In addition to the ionization, charged particles passing through the argon produce approximately 24,000 scintillation photons per MeV. The scintillation photons are fast, arriving at the photon detectors (PDs) nanoseconds after production. This scintillation light provides a t_0 for each event. Comparison of the arrival time of ionization at the anode with this t_0 enables reconstruction in the drift direction. The SP module implementation enables $\sim$1 mm position resolution for 10 MeV SNB events. The PD t_0 is also vital in fiducializing nucleon decay events, which allows us to reject cosmic-muon-induced background events that will occur near the edges of the detector modules.

The photons are collected by devices called X-ARAPUCAs, which are mounted in the APA frames between the sets of wire layers, as shown in Figure 1.3. The X-ARAPUCAs consist of layers of dichroic filter and wavelength-shifter, illustrated in Figure 1.5, that shift the VUV scintillation light into the visible range trap the visible photons, and transport them to silicon photomultiplier (SiPM) devices. The signals from these SiPMs are sent along cables that pass through the hollow APA frames, up to feedthroughs in the cryostat roof. The PD and APA-wire data-streams are merged at the DAQ.

PD modules, shown in Figure 1.6, are 209 cm × 12 cm × 2 cm bars that each hold 24 X-ARAPUCAs. Ten PD modules are mounted in each APA between the wire layers.

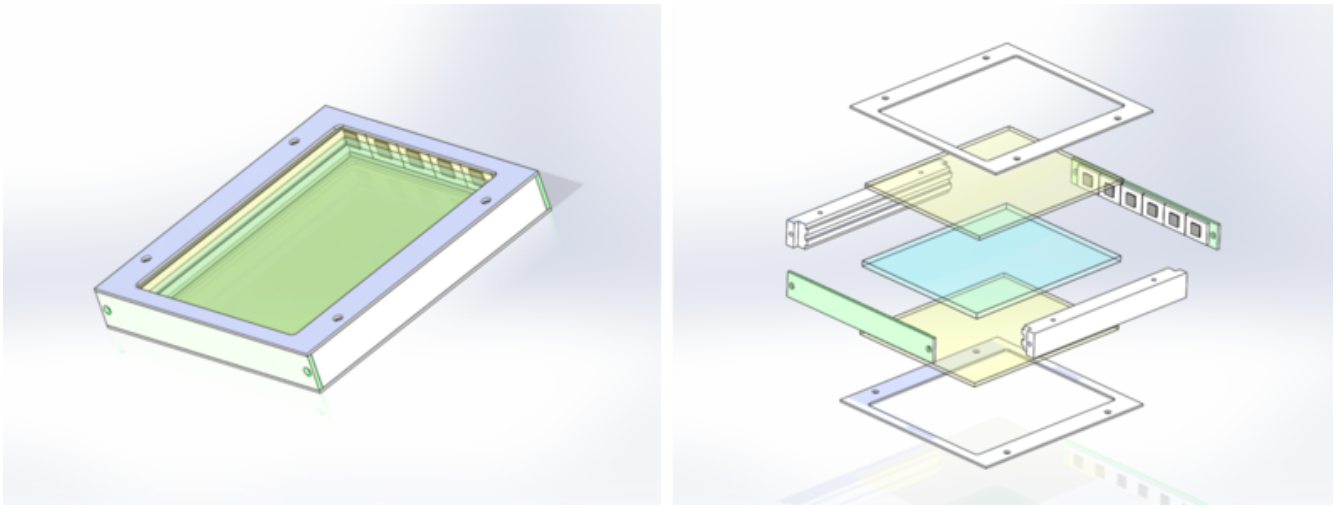


Figure 1.5: Left: an X-ARAPUCA cell. Right: an exploded view of the X-ARAPUCA cell, where the blue sheet is the wavelength-shifting (WLS) plate and the yellow sheets are the dichroic filters.

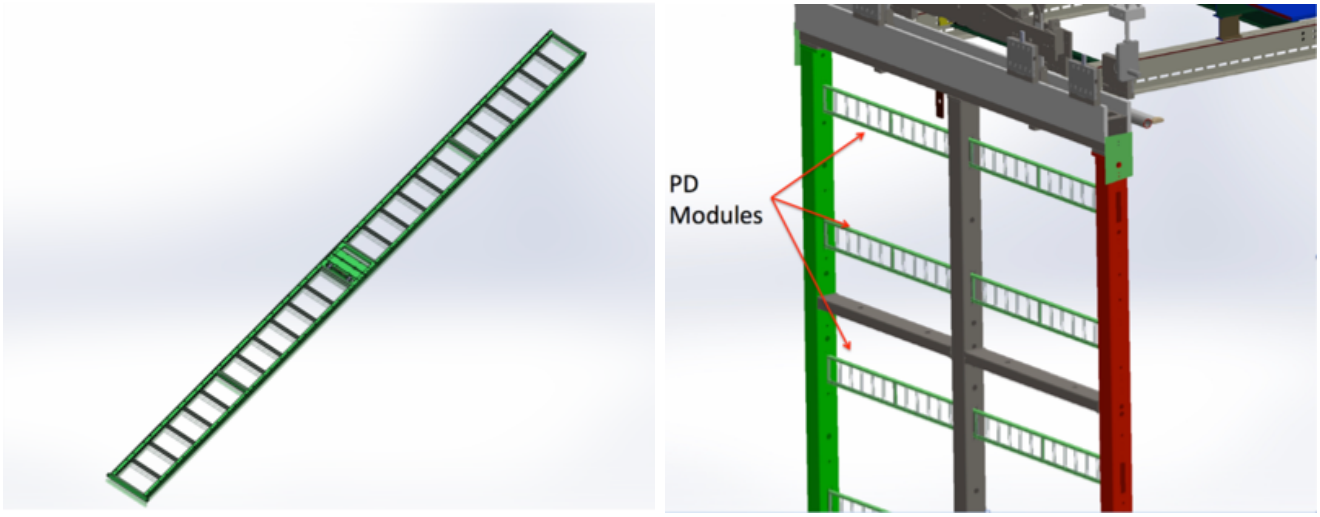


Figure 1.6: Left: an X-ARAPUCA PD module. The 48 SiPMs that detect the light from the 24 cells are along the long edges of the module. Right: X-ARAPUCA PD modules mounted inside an APA.

The 48 SiPMs on each X-ARAPUCA supercell are ganged together, and the signals are collected by FE electronics, mounted on the supercell. The design of the FE electronics is inspired by the system used for the Mu2e cosmic-ray tagger [2], which uses commercial ultrasound ASICs. The FE electronics define the 1 µs timing resolution of the PD system.

1.6 Calibration

The challenge of calibrating the DUNE FD is controlling the response of a huge cryogenic detector over a period of decades, a challenge amplified by the detector's location deep underground and therefore shielded from the cosmic muons that have typically been used as standard candles for LArTPCs. The FD calibration system has been designed jointly for the SP and dual-phase (DP) technologies, and uses the same strategies and systems for both.

To achieve our GeV-scale oscillation and nucleon decay physics goals, we must know our fiducial volume to 1 – 2% and have a similar understanding of the vertex position resolution; understand the ν_e event rate to 2%; and control our lepton energy scales to 1% and hadron energy scales to 3%. At the MeV scale, our physics requirements are driven by our goal of identifying and measuring the spectral structure of an SNB; here, we must achieve a 20 – 30% energy resolution, understand our event timing to the 1 µs level, and measure our trigger efficiency and levels of radiological background.

The tools available to us for calibration include the LBNF beam, atmospheric neutrinos, atmospheric muons, radiological backgrounds, and dedicated calibration devices installed in the detector. At the lowest energies, we have deployable neutron sources and intrinsic radioactive sources; in particular, the natural ^{39}Ar component of the LAr with its 565 keV end-point, given its pervasive nature across the detector, can be used to measure the spatial and temporal variations in electron lifetime. The possibility of deploying radioactive sources is also under study. In the 10 MeV to

100 MeV energy range, we will use Michel electrons, photons from π^0 decay, stopping protons, and both stopping and through-going muons. We will also have built-in lasers, purity monitors, and thermometers, as well as the ability to inject charge into the readout electronics. Finally, data from the ProtoDUNE detectors (Section **??**) will be invaluable in understanding the response and particle ID (PID) capabilities of the FD.

Over time, the FD calibration program will evolve as statistics from cosmic rays and the LBNF beam amass and add to the information gained from the calibration hardware systems. These many calibration tools will work alongside the detector monitoring system, the computational fluid dynamics (CFD) models of the argon flow, and ProtoDUNE data to give us a detailed understanding of the FD response across the DUNE physics program.

1.7 Data Acquisition

The DAQ systems for the SP and DP technologies have been designed jointly and are identical except for the architecture of the detector readout electronics. The output format of the generated data is common, and both are synchronized to the same global clock signals. The DAQ architecture is based on the Front-End Link eXchange (FELIX) system designed at CERN and used for the LHC experiments.

The DAQ is divided between an upstream section, located underground in the CUC, and a downstream DAQ back-end subsystem (DAQ BE) to be located above ground at the Sanford Underground Research Facility (SURF). All trigger decisions are made upstream, and the data is buffered underground until the DAQ BE indicates it is ready to receive data; this controls the rate of data flowing to the surface. An end-goal of the DAQ is to achieve a data rate to tape of no more than 30 PB/year.

For the SP module, the 150 APAs are processed by 75 DAQ readout units (DAQ RUs); each DAQ RU contains one FELIX board. The PDs from the module will have a lower data rate because the PD electronics, unlike the TPC electronics, perform zero-suppression; therefore, the PDs of a module will be processed by six to eight additional DAQ RUs. The DAQ can be partitioned: it will be possible to run multiple instances of the DAQ simultaneously, so most of the detector can be taking physics data while other DAQ instances are doing test runs for development or special runs such as calibration runs.

Two basic triggers will be operating. Beam, cosmic, and nucleon decay events will be triggered using the localized high-energy trigger that will open a readout window of 5.4 ms, enough to read out the full TPC drift around an event. For SNBs, we will use an extended low-energy trigger. This will look for coincident regions of low-energy deposits, below 10 MeV, across an entire module and in a 10 s period. An extended high-energy trigger will open a readout window of 100 s to capture a full SNB.

The DAQ must also provide the system clock that keeps the detector components synchronized and timestamps all data. The timestamp derives from a Global Positioning System (GPS) one-

pulse-per-second signal (1PPS signal) fed into the DAQ with 1 µs precision, adequate for beam and SNB events. To provide finer synchronization between detector components, a 10 MHz reference clock drives the module's 62.5 MHz master clock, which is fanned out to all detector components, providing an overall synchronization to a precision of 1 ns.

1.8 Cryogenics Instrumentation and Slow Controls

DUNE's cryogenic instrumentation and slow controls (CISC) system is responsible for recognizing and preventing fault conditions that could develop in a detector module over long periods of running. The SP and DP modules will use a CISC system that has been designed jointly.

Cryogenics instrumentation includes purity monitors, various types of temperature monitors, and cameras with their associated light emitting systems. Also included are gas analyzers and LAr level monitors that are directly related to the external cryogenics system, which have substantial interfaces with LBNF.

Cryogenics instrumentation requires significant engineering, physics, and simulation work, such as E field simulations and cryogenics modeling studies using computational fluid dynamics (CFD). E field simulations identify desirable locations for instrumentation devices in the cryostat, away from regions of high E field, so that their presence does not induce large field distortions. CFD simulations help identify expected temperature, impurity, and velocity flow distributions and guide the placement and distribution of instrumentation devices inside the cryostat.

The slow controls portion of CISC consists of three main components: hardware, infrastructure, and software. The slow controls hardware and infrastructure comprises networking hardware, signal processing hardware, computing hardware, and associated rack infrastructure. The slow controls software provides, for every slow control quantity, the central slow controls processing architecture, databases, alarms, archiving, and control room displays.

1.9 Installation

A significant challenge for DUNE is transporting all detector and infrastructure components down the 1500 m Ross shaft and through drifts to a detector cavern. The 150 anode plane assemblies, each 6.0 m high and 2.3 m wide, and weighing 600 kg with 3500 strung sense and shielding wires, must be taken down the shaft as special "slung loads," presenting an extra challenge.

Once the SP module cryostat is ready, a temporary construction opening (TCO) is left open at one end through which the detector components are installed. A cleanroom is built around the TCO to prevent any contamination entering the cryostat during installation. The detector support system (DSS) is then installed into the cryostat, ready to receive the TPC components.

In the cleanroom the APAs are outfitted with PD units and passed through a series of qualification tests. Two APAs are linked into a vertical 12 m high double unit and connected to readout electronics. They are tested in a cold box, then move into the cryostat to be installed at the proper location on the DSS, and have their cabling connected to feedthroughs. The FC, cathode plane assemblies and their HV connections, elements of the CISC, and detector calibration systems are installed in parallel with the APAs.

After twelve months of detector component installation, the TCO closes (the last installation steps occur in a confined space accessed through a narrow human-access port on top of the cryostat). Following leak checks, final electrical connection tests, and installation of the neutron calibration source, the process of filling the cryostat with 17,000,000 kg of LAr begins.

To help plan the installation phase, installation tests will be performed at the NOvA FD site in Ash River, Minnesota, USA. These tests will allow us to develop our procedures, train installation workers, and develop our labor planning through time and motion studies. Throughout the project, safety, quality assurance (QA), and quality control (QC) are written into all processes.

Safety of both personnel and detector components is the paramount consideration throughout the installation process and beyond. Once the detectors are taking data, the DUNE detector safety system (DDSS) will be monitoring for argon level drops, water leaks, and smoke. A detailed detector and cavern grounding scheme has been developed that not only guards against ground loops but also ensures that any power faults are safely shunted to the facility ground.

Glossary

one-pulse-per-second signal (1PPS signal) An electrical signal with a fast rise time and that arrives in real time with a precise period of one second. 10

analog-to-digital converter (ADC) A sampling of a voltage resulting in a discrete integer count corresponding in some way to the input. 8

anode plane assembly (APA) A unit of the SP detector module containing the elements sensitive to ionization in the LAr. It contains two faces each of three planes of wires, and interfaces to the cold electronics and photon detection system. 3, 5–12

Ash River The Ash River, Minnesota, USA NOvA experiment far site, used as an assembly test site for Deep Underground Neutrino Experiment (DUNE). 12

ASIC application-specific integrated circuit. 7, 9

charged current (CC) Refers to an interaction between elementary particles where a charged weak force carrier (W^+ or W^-) is exchanged. 2, 3

cold electronics (CE) Analog and digital readout electronics that operate at cryogenic temperatures. 5, 7, 8

computational fluid dynamics (CFD) High performance computer-assisted modeling of fluid dynamical systems. 10, 11

cryogenic instrumentation and slow controls (CISC) Includes equipment to monitor all detector components and liquid argon (LAr) quality and behavior, and provides a control system for many of the detector components. 11, 12

cathode plane assembly (CPA) The component of the SP detector module that provides the drift HV cathode. 3, 7, 12

charge-parity symmetry violation (CPV) Lack of symmetry in a system before and after charge and parity transformations are applied. For CP symmetry to hold, a particle turns into its corresponding antiparticle under a charge transformation, and a parity transformation

inverts its space coordinates, i.e., produces the mirror image. 2

central utility cavern (CUC) The utility cavern at the 4850L of Sanford Underground Research Facility (SURF) located between the two detector caverns. It contains utilities such as central cryogenics and other systems, and the underground data center and control room. 7, 10

data acquisition (DAQ) The data acquisition system accepts data from the detector front-end (FE) electronics, buffers the data, performs a trigger decision, builds events from the selected data and delivers the result to the offline secondary DAQ buffer. 7, 8, 10, 11

DAQ back-end subsystem (DAQ BE) The portion of the data acquisition (DAQ) that is generally toward its output end. It is responsible for accepting and executing trigger commands and marshaling the data they address to output storage buffers. 10

DAQ readout unit (DAQ RU) The first element in the data flow of the DAQ. 10

DUNE detector safety system (DDSS) The system used to manage key aspects of detector safety. 12

detector module The entire DUNE far detector is segmented into four modules, each with a nominal 10 kt fiducial mass. 7, 11

dual-phase (DP) Distinguishes one of the DUNE far detector technologies by the fact that it operates using argon in both gas and liquid phases. 9, 10

DP module dual-phase DUNE far detector (FD) module. 11

detector support system (DSS) The system used to support a single-phase (SP) detector module within its cryostat. 11, 12

Deep Underground Neutrino Experiment (DUNE) A leading-edge, international experiment for neutrino science and proton decay studies. 2, 9–11

field cage (FC) The component of a liquid argon time-projection chamber (LArTPC) that contains and shapes the applied E field. 7, 12

far detector (FD) The 70 kt total (40 kt fiducial) mass LArTPC DUNE detector, composed of four 17.5 kt total (10 kt fiducial) mass modules, to be installed at the far site at SURF in Lead, SD, USA. 4, 7, 9, 10, 12

front-end (FE) The front-end refers a point that is "upstream" of the data flow for a particular subsystem. For example the SP front-end electronics is where the cold electronics meet the sense wires of the TPC and the front-end DAQ is where the DAQ meets the output of the electronics. 7–9

Front-End Link eXchange (FELIX) A high-throughput interface between FE and trigger elec-

tronics and the standard PCIe computer bus. 10

Global Positioning System (GPS) A satellite-based system that provides a highly accurate one-pulse-per-second signal (1PPS signal) that may be used to synchronize clocks and determine location. 10

grand unified theory (GUT) A class of theories that unifies the electro-weak and strong forces. 2

high voltage (HV) Generally describes a voltage applied to drive the motion of free electrons through some media, e.g., LAr. 7, 12

liquid argon (LAr) Argon in its liquid phase; it is a cryogenic liquid with a boiling point of $-90\,^{\circ}\mathrm{C}$ (87 K) and density of 1.4 g/ml. 2, 3, 7, 9, 11, 12

liquid argon time-projection chamber (LArTPC) A time projection chamber (TPC) filled with liquid argon; the basis for the DUNE FD modules. 2, 3, 9

Long-Baseline Neutrino Facility (LBNF) The organizational entity responsible for developing the neutrino beam, the cryostats and cryogenics systems, and the conventional facilities for DUNE. 2, 9–11

LHC Large Hadron Collider. 10

minimum ionizing particle (MIP) Refers to a particle traversing some medium such that the particle's mean energy loss is near the minimum. 7

Mu2e An experiment sited at Fermi National Accelerator Laboratory (Fermilab) that searches for charged-lepton flavor violation and seeks to discover physics beyond the standard model (SM). 9

NOvA The NOvA off-axis neutrino oscillation experiment at Fermilab. 12

photon detector (PD) The detector elements involved in measurement of the number and arrival times of optical photons produced in a detector module. 3, 6, 8–10, 12

particle ID (PID) Particle identification. 10

parts per million (ppm) A concentration equal to one part in 10^{-6}. 3

parts per trillion (ppt) A concentration equal to one part in 10^{-12}. 3

ProtoDUNE Either of the two DUNE prototype detectors constructed at European Organization for Nuclear Research (CERN). One prototype implements SP technology and the other dual-phase (DP). 10

ProtoDUNE-SP The SP ProtoDUNE detector at CERN. 5

quality assurance (QA) The set of actions taken to provide confidence that quality requirements are fulfilled, and to detect and correct poor results. 12

quality control (QC) An aggregate of activities (such as design analysis and inspection for defects) performed to ensure adequate quality in manufactured products. 12

signal-to-noise (S/N) signal-to-noise ratio. 3, 5

silicon photomultiplier (SiPM) A solid-state avalanche photodiode sensitive to single photoelectron signals. 8, 9

standard model (SM) Refers to a theory describing the interaction of elementary particles. 2

supernova neutrino burst (SNB) A prompt increase in the flux of low-energy neutrinos emitted in the first few seconds of a core-collapse supernova. It can also refer to a trigger command type that may be due to this phenomenon, or detector conditions that mimic its interaction signature. 2, 3, 7–11

single-phase (SP) Distinguishes one of the DUNE far detector technologies by the fact that it operates using argon in its liquid phase only. 2, 3, 9–11

SP module single-phase DUNE FD module. 3, 8, 10, 11

Sanford Underground Research Facility (SURF) The laboratory in South Dakota where the Long-Baseline Neutrino Facility (LBNF) far site conventional facilities (FSCF) will be constructed and the DUNE FD will be installed and operated. 10

temporary construction opening (TCO) An opening in the side of a cryostat through which detector elements are brought into the cryostat; utilized during construction and installation. 11, 12

time projection chamber (TPC) A type of particle detector that uses an E field together with a sensitive volume of gas or liquid, e.g., LAr, to perform a 3D reconstruction of a particle trajectory or interaction. The activity is recorded by digitizing the waveforms of current induced on the anode as the distribution of ionization charge passes by or is collected on the electrode. 7, 10, 11

VUV vacuum ultra-violet. 3, 8

warm interface board (WIB) Digital electronics situated just outside the SP cryostat that receives digital data from the front-end mother boards (FEMBs) over cold copper connections and sends it to the reconfigurable computing element (RCE) FE readout hardware. 7

wavelength-shifting (WLS) A material or process by which incident photons are absorbed by a material and photons are emitted at a different, typically longer, wavelength. 8

X-ARAPUCA Extended ARAPUCA design with wavelength-shifting (WLS) coating on only the external face of the dichroic filter window(s) but with a WLS doped plate inside the cell. 8, 9

References

[1] C. Rubbia, "The Liquid Argon Time Projection Chamber: A New Concept for Neutrino Detectors," Tech. Rep. CERN-EP-INT-77-08, 1977.

[2] **Mu2e** Collaboration, L. Bartoszek *et al.*, "Mu2e Technical Design Report," arXiv:1501.05241 [physics.ins-det].